MNRAS **451,** 804–812 (2015) doi:10.1093/mnras/stv892

A debris disc under the influence of a wide planetary-mass companion: the system of HD 106906

Lucie Jílková★ and Simon Portegies Zwart

Leiden Observatory, Niels Bohrweg 2, Leiden, NL-2333 CA, the Netherlands

Accepted 2015 April 19. Received 2015 April 17; in original form 2014 July 2

ABSTRACT

The 13-Myr old star HD 106906 is orbited by a debris disc of at least 0.067 M_{Moon} with inner and outer radii of 20 and 120 au, respectively, and by a planet at a distance of 650 au. We use this curious combination of a close low-mass disc and a wide planet to motivate our simulations of this system. We study the parameter space of the initial conditions to quantify the mass loss from the debris disc and its lifetime under the influence of the planet. We find that when the planet orbits closer to the star than about 50 au and with low inclination relative to the disc (less than about 10°), more disc material is perturbed outside than inside the region constrained by observations on time-scales shorter than 1 Myr. Considering the age of the system, such a short lifetime of the disc is incompatible with the time-scale for planet–planet scattering, which is one of the scenarios suggested to explain the wide separation of the planet. For some configurations, when the planet orbit is inclined with respect to the disc, the latter will start to wobble. We argue that this wobbling is caused by a mechanism similar to Kozai–Lidov oscillations. We also observe various resonant structures (such as rings and spiral arms) induced in the disc by the planet.

Key words: celestial mechanics – planets and satellites: formation – planets and satellites: individual: HD 106906 b – planet–disc interactions – circumstellar matter – open clusters and associations: individual: Lower Centaurus Crux.

1 INTRODUCTION

About a dozen planetary-mass companions at wide separations of about 50–100 au from their host stars have been revealed by direct imaging surveys during the past decade (Kraus et al. 2014) and several cases were observed at separations of 150–300 au (e.g. Lafreniere, Jayawardhana & van Kerkwijk 2008; Kraus et al. 2014). Moreover, two recent discoveries report companions located as far as ∼650 au (Bailey et al. 2014) and ∼2000 au (Naud et al. 2014). The origin of such wide planetary-mass companions is not well understood and presents important constraints on our general understanding of planet formation. Several scenarios have been proposed and, depending on the eccentricity and separation of the planet, the environment in which the system evolves and the time-scale of formation, two main mechanisms are usually considered.

In situ formation by core accretion (e.g. Rafikov 2011) or protoplanetary disc fragmentation (e.g. Boss 2011; Vorobyov 2013) can explain part of the observed population of wide-orbit planets but is unlikely to be the only formation channel (see also Veras, Crepp & Ford 2009; D'Angelo, Durisen & Lissauer 2011; Chabrier et al. 2014, for recent reviews of the topic).

Another explanation argues that the planet formed closer to the parent star in the protoplanetary disc and was scattered outward by dynamical interaction with another planet in the system or with a perturbation of external origin (see e.g. Davies et al. 2014 for a summary on various interactions in planetary systems). Given the diversity of the observed wide planetary systems and the environment they are expected to form in, the parameter space for the initial conditions of such scattering events is extremely large and complex. The formation can involve, for example, stellar flybys (e.g. Malmberg, Davies & Heggie 2011), exchange interactions (Portegies Zwart & McMillan 2005), planetary migration (e.g. Crida, Masset & Morbidelli 2009) and scattering in a multiple planetary system (Scharf & Menou 2009), dynamical interaction between circumstellar discs and planets (see Baruteau et al. 2014, for a recent summary), the effects of Galactic tides (e.g. Veras & Evans 2013), recapture of free-floating planets (Perets & Kouwenhoven 2012) or a combination of these interactions (Raymond, Armitage & Gorelick 2010; Boley, Payne & Ford 2012; Hao, Kouwenhoven & Spurzem 2013). Studying specific objects narrows down this parameter space, since some of the characteristics are constrained by observations.

In this context, we focused on HD 106906, which is an F5–V star with a debris disc (Chen et al. 2005, 2011) and a planetary-mass companion at a distance of about 650 au (Bailey et al. 2014). The chance of coincidental projection of the star and planet is negligible

★ E-mail: jilkova@strw.leidenuniv.nl

and therefore the observed distance between the star and planet is interpreted as an orbital separation. Irrespective of the inclination of the planetary orbit, which is unknown, the observed separation must be part of the orbit, which makes it one of the widest separations ever observed.

Regardless of the process that caused this planet to have such a wide orbit, the observed debris disc has survived. The lifetime of the debris disc as observed constrains how long ago the current configuration formed. In this article, we study the time-scale on which the disc erodes due to the influence of the planet and use this time-scale to constrain the mechanism that delivered the planet in its extremely wide orbit. We carry out simulations of the evolution of the disc under the influence of the planet, taking the observed characteristics of the system as the initial conditions. We vary the inclination of the disc with respect to the planetary orbit and the pericentre distance of the planet (i.e. its eccentricity under the assumption that the apocentre distance of the orbit is 650 au) within the observational constraints and we explore the erosion time-scale of the disc due to the planet.

1.1 The HD 106906 system

HD 106906 (also known as HIP 59960) belongs to the Lower Centaurus Crux (LCC) group, which is a subgroup of the Scorpius–Centaurus (ScoCen) OB association (de Zeeuw et al. 1999). The host star, called HD 106906 A, is classified as an F5–V star. Pecaut, Mamajek & Bubar (2012) measured the median age of the LCC group as 17 ± 1 Myr and the mass and age for HD 106906 A as $M_\star = 1.5\,\mathrm{M}_\odot$ and 13 ± 2 Myr, respectively. In Table 1, we summarize the observed data and derived characteristics of the HD 106906 system.

The observed infrared (IR) spectral energy distribution of HD 106906 A shows a strong excess that indicates the presence of a debris disc with an inner cavity. Chen et al. (2011, see also Chen et al. 2005 for the initial results based on the same observational data) obtained broad-band observations of HD 106906 with the Multiband Imaging Photometer for *Spitzer* at 24 and 70 μm. By fitting these excess fluxes with a single blackbody, they derived the disc's colour temperature of 93 K and fractional IR luminosity with respect to the star of $L_{\rm IR}/L_\star = 1.3 \times 10^{-3}$. Bailey et al. (2014) confirmed these results using additional *Spitzer* data up to ∼100 μm, obtaining a disc temperature of 95 K.

Table 1. Characteristics of the HD 106906 system.

Characteristic	Value	Unit	Ref.
Distance	92 ± 2	pc	*a*
Age	13 ± 2	Myr	*b*
HD 106906 A			
Spectral type	F5V		*b*
Mass $M_\star$	1.5 ± 0.1	$\mathrm{M}_\odot$	*b*
Luminosity $L_\star$	5.6 ± 0.8	$\mathrm{L}_\odot$	*b*
Temperature	6516 ± 165	K	*b*
HD 106906 b			
Mass M_b	11 ± 2	$\mathrm{M}_{\rm Jup}$	*c*
Separation R_b	650 ± 40	au	*c*
disc			
24-μm flux density	103.1 ± 2.5	mJy	*d*
70-μm flux density	281 ± 28	mJy	*d*
Fractional luminosity $L_{\rm IR}/L_\star$	1.3×10^{-3}		*d*
Dust grain temperature	95	K	*c*
Inner radius	∼20	au	*c*
Outer radius	<120	au	*c*
Minimum mass	0.067	$\mathrm{M}_{\rm Moon}$	*d*

References: *a* – van Leeuwen (2007), *b* – Pecaut et al. (2012); *c* – Bailey et al. (2014); *d* – Chen et al. (2011).

The disc around HD 106906 A is expected to be optically thin. Chen et al. (2011) identified 55 stars with an IR excess in their sample of 167 ScoCen OB Association members of intermediate age (10–30 Myr) and F, G, or K spectral types. They did not find any significant difference in the distribution of the IR excess (measured by the $L_{\rm IR}/L_\star$ ratio) for fast and slow rotating stars. As a difference in rotation speed is expected for stars hosting gas-rich and gas-poor stars (due to magnetic braking, e.g. Rebull et al. 2006), it is likely that the stars in the ScoCen association have optically thin and gas-poor discs.

Since the disc is not resolved at any wavelength, its characteristic extent can be estimated from the temperature. Assuming the dust grains are blackbodies in radiative equilibrium with the central star, forming an optically thin disc with grains of constant size and chemical composition, Chen et al. (2011) derived a single grain distance of about 34 au. Based on the comparison with *Herschel* observations of a sample of resolved circumstellar discs, Bailey et al. (2014) further estimated the extent of the disc to be about 20–120 au (for the optically thin disc). Chen et al. (2011) also estimated a minimum dust-grain size of 1.4 μm and a minimum mass of IR-emitting dust grains of $0.067\,\mathrm{M}_{\rm Moon}$.

The planetary-mass companion of HD 106906, called HD 106906 b, was discovered by Bailey et al. (2014) with the Magellan Adaptive Optics/Clio2 system. They obtained resolved images of the companion, confirming that the planet is comoving with the host star, and classified its spectral type as L2.5±1. As mentioned above, the projected separation between the host star and the companion is then 650 au. Using evolutionary models for an object of this spectral type and age corresponding to the one of the LCC group, Bailey et al. (2014) further estimated the mass of the planet to be $M_\mathrm{b} = 11 \pm 2\,\mathrm{M}_{\rm Jup}$. The properties of the planet make the formation of HD 106906 difficult to explain. The two most compelling formation mechanisms for the origin of planets in wide orbits are discussed by Bailey et al. (2014): (i) *in situ* formation at a large separation, as wide as the orbital separation found in some binary stars, and (ii) formation in a tight orbit and subsequent scattering to the current wide orbit. The mass ratio $M_\mathrm{b}/M_\star \sim 0.01$ is unusually small for the first suggested mechanism. In the later scenario, a perturber must have been present in order to move the planet to its current orbit. This culprit, however, may be long gone, lost in interstellar space. This is consistent with the lack of another massive planet in the system (Bailey et al. 2014) – no other object is detected within the observational limits, which translates to a mass no greater than M_b beyond 35 au and a mass no greater than 5–7 $\mathrm{M}_{\rm Jup}$ beyond 70 au. We cannot rule out other formation mechanisms, such as the possible capture of the planet from the surrounding environment in the LCC group.

Here we explore the lifetime of the current configuration of the system. Planet–planet scattering is predicted to occur after the dissipation of the gas from the circumstellar disc at about 10^5 yr (see e.g. Chatterjee et al. 2008, and references therein). Planets at wide separation (>100 au) are estimated to be most probably produced on time-scales up to 10^7 yr (e.g. Veras et al. 2009; Scharf & Menou 2009). If the current planetary orbit is the result of a scattering interaction with another planet, both planets once orbited the parent star in much closer orbits, probably within the observed inner edge of the disc. The current planetary orbit must still bear the memory of that original orbit and the place where the scattering happened,

closer to the parent star, should also be part of the orbit. The lifetime of the disc under the influence of such a planet should then be at least a few Myr in order to be consistent with the lifetime of the system.

We investigate the mass loss of the disc for different eccentricities and inclinations of the orbit with respect to the disc.

2 SIMULATIONS

We performed simulations of the evolution of the system starting with initial conditions corresponding to its current observed characteristics (see Table 1). We varied some of the unconstrained properties, namely the pericentre of the planetary orbit, R_p, and the inclination of the disc, i, since these can in principle be random, depending on the formation process of the system.

2.1 Method

We calculated the orbit of the star–planet system independently of the evolution of the disc. Since the mass of the disc is small compared with the planet or star, we represented the disc by a number of zero-mass particles – planetesimals – and hence we do not take the self-gravity of the disc into account.

All calculations were carried out within the Astrophysical Multipurpose Software Environment (AMUSE:[1] Portegies Zwart et al. 2013; Pelupessy et al. 2013). We used N-body integrator HUAYNO (Pelupessy, Jänes & Portegies Zwart 2012) to calculate the orbit of the star–planet system. The orbits of the disc particles were calculated by solving Kepler's equations using universal variables (adopted from the SAKURA code: Gonçalves Ferrari, Boekholt & Portegies Zwart 2014). The implementation of the solver in AMUSE allows us to integrate Keplerian orbits efficiently in the potential of a central star with a number of orbiters (i.e. planetesimals orbiting the star in our case). Our approach is not self-consistent – the planet and star are not influenced by the planetesimals in the disc. The gravitational influence of the planet is coupled with the planetesimals. This coupling, called *Bridge* (Fujii et al. 2007), is an extension of the mixed-variable symplectic scheme developed by Wisdom & Holman (1991) and it is used here to couple different dynamical regimes within one self-gravitating system (i.e. the planetesimal debris disc and the planet orbiting the central star). The time complexity of our numerical scheme is $\propto N$, rather than the usual $\propto N^2$ for a direct N-body approach. The implementation of Bridge in AMUSE is described in Pelupessy et al. (2013).

The symplectic mapping method of Wisdom & Holman (1991) was first applied to calculate the long-term evolution the Solar system and has since been widely used to simulate the evolution of planetary systems in general, including interaction with planetesimals. Fragmenting planetesimals are generally considered to be the parent bodies of the dust that is observed as a debris disc (e.g. Wyatt 2008) and complex methods have been developed to model this process accurately (see e.g. Thébault 2012, and references therein). The planetesimal disc approximation is often used to define the spatial and velocity distributions of the dust particles. For example, Larwood & Kalas (2001) investigated the affect of stellar flybys on the structure of the debris disc observed in the β Pictoris system and similarly in Chiang et al. (2009) for the Fomalhaut system. Wyatt (2003) and Reche et al. (2008) studied the resonant trapping of planetesimals due to planetary migration. Lestrade et al. (2011) investigated the stripping of the planetesimal debris disc by a close stellar flyby. Long-lived asymmetric structures were simulated by, e.g. Faramaz et al. (2014, eccentric debris disc around ζ^2 Reticuli) and Pearce & Wyatt (2014, more general case of a planet within the outer edge of the disc).

We tested the method by comparing our implementation with direct N-body integrations, which gave the same results both qualitatively and quantitatively; we successfully reproduced the results of Lestrade et al. (2011).

2.2 Numerical set-up and initial conditions

Following the observations, we assumed a mass of 1.5 $M_\odot$ for the star and 11 M_{Jup} for the planet (see Section 1.1 and Table 1). The apocentre distance of the planet was 650 au in all our simulations. This is the observed separation, which we assume to be the apocentre of the orbit and which is the planet's initial position in our simulations. The pericentre distance of the planet, R_p, had values ranging from 1–650 au, corresponding to orbital eccentricities of 0.997 and a circular orbit, respectively (see Table 2 for the list of all pericentre values considered). The orbit of the planet was integrated with HUAYNO using the hold drift–kick–drift integrator. The HUAYNO integrator uses individual time steps that are proportional to interparticle free-fall times and the coefficient of the proportionality is called η. We chose different values of η for different pericentres (i.e. orbital eccentricities), so that the energy conservation of the star–planet system is always at 10^{-6} level and lower; this level of energy conservation turns out to be very conservative (Portegies Zwart & Boekholt 2014). The values of η are specified in Table 2 for each orbital configuration.

Disc planetesimals begin in an initially uniform random distribution in radius between the inner and outer disc radii of 20 and 120 au, respectively, which corresponds to the values estimated from observations (see Section 1.1 and Table 1). Such a choice of radial distribution corresponds to a surface density profile $\propto 1/r$, where r is the radial distance to the star, which is often used to model protoplanetary discs (see e.g. Steinhausen, Olczak & Pfalzner 2012, and references therein) and is supported by observations (e.g. Andrews & Williams 2007). Following the discussion in Steinhausen et al. (2012), we tested how our results depend on the chosen initial surface density profile. Since the disc is represented by test particles (i.e. its self-gravity is not taken into account), different surface density profiles can be taken into account in the post-processing of the simulations. We considered a surface density profile $\propto 1/r^{1.5}$, corresponding to the Minimum Mass Solar Nebula (Hayashi 1981), and found that such a profile changes the disc fractions presented in Section 3.1 by less than 10 per cent.

Table 2. Planetary pericentres and time steps for the integrations.

R_p [au]	η	t_{BR}[a]
1	0.001	0.001
10	0.001	0.002
20, 30, 40, 50, 60	0.001	0.01
70, 80, 90, 100, 110	0.001	0.05
120, 150, 200, 350, 500, 650	0.003	0.05

Notes. [a]The Bridge time-step, t_{BR}, is given in units of the period of the circular orbit at 20 au from the star, which is 73 yr.

[1] http://amusecode.org

The planetesimals are initially placed in one plane with a random, uniform azimuthal distribution and have circular orbits. The inclination of the disc with respect to the planetary orbit, i, has values between 0° and 180°, where $i = 0°$ corresponds to the coplanar prograde case and $i = 180°$ corresponds to the coplanar retrograde case. The disc plane is rotated around an axis perpendicular to the semimajor axis of the planetary orbit. Each simulation was carried out with 10^4 particles, but we confirmed that increasing this number to 10^5 does not change the results. Decreasing the number to 10^3 particles gives qualitatively similar results, but the smaller number of particles makes post-processing analysis harder, due to the lower statistics.

The planetesimals feel the gravitational force from the planet with the specific time step of the interaction, $t_{\rm BR}$ – the Bridge time-step – which is the time step over which the system integrates the combined solver. The time step differs for different initial conditions of the planetary orbit: for more eccentric planetary orbits, we adopted a shorter time step. $t_{\rm BR}$ has values ranging from 10^{-3} to 5×10^{-2} of the orbital period of the initial inner disc edge of 73 yr. The values of $t_{\rm BR}$ are specified in Table 2 for each orbital configuration. We verified the choice of $t_{\rm BR}$ by comparing the integrations using Bridge with the calculations where the whole system was treated by the N-body code. These control N-body simulations were carried with 10^3 zero-mass particles in the disc. We used the HUAYNO integrator in AMUSE with a choice of η giving energy conservation of order 10^{-6} or lower. To treat close encounters of planetesimals with the star, we use Plummer softening with smoothing length $\epsilon = 0.001$ au $= 0.2\,{\rm R}_\odot$. The results of the direct and our Bridged direct–Kepler solver are in good agreement. More quantitatively, we compared the disc fraction, $f_{\rm d/b}$ – the main output of our simulations defined in Section 3.1 – which generally agrees at a ∼5 per cent level.

3 RESULTS

In Fig. 1, we show an example of our simulation: the configuration with a pericentre of 20 au (at the inner edge of the disc) and a disc inclination of 5°. The surface number densities of planetesimals in the plane of the planetary orbit (xy) and the edge-on plane (xz) are plotted in the upper and lower panels, respectively. As the planet plunges through the disc, it perturbs the planetesimal orbits and the disc is disrupted. Some planetesimals move outside the initial disc region and some become unbound from the star and escape from the system. The majority of particles that are moving outside the initial disc region are perturbed farther away from the star, i.e. their semimajor axis is larger than the outer disc radius of 120 au (indicated by the grey ellipse in Fig. 1) and only a small fraction of particles orbit within the inner disc edge (with semimajor axis smaller then 20 au). Note that we do not consider collisions between the planetesimals themselves, either with the star or with the planet, and no particles are removed from the simulation.

3.1 Parameter-space study

We explored the parameter space of the pericentre of the planetary orbit ($R_{\rm p}$) and the inclination of the disc with respect to the orbital plane (i). In Fig. 2, we show the fraction of disc particles that stay bound to the star after 1 Myr of evolution, $n_{\rm bound}/n_{\rm tot}$, where $n_{\rm bound}$ is the number of bound particles and $n_{\rm tot}$ is the total number (i.e. $n_{\rm tot} = 10^4$). Fig. 2 maps the prograde cases ($0° < i \leq 90°$); the results for the retrograde configurations are generally similar (see below for some examples). We see that only in the coplanar case, when the pericentre is smaller that the outer disc radius, is a substantial number of particles lost (unbound) from the system. It is hardly surprising that the highest number of unbound particles is produced in such configurations, but it is interesting that more than ∼80 per cent of the particles stay bound for all other considered configurations during the first 1 Myr.

The number of bound particles measures what part of the original disc is kept within the system which, however, does not correspond directly to the observed disc. For example, in the second and the last snapshots of Fig. 1, we see that a substantial number of planetesimals are located outside the disc area as it was constrained from the observations. Most of these planetesimals are, however, still bound to the star and the ratio $n_{\rm bound}/n_{\rm tot}$ is about 0.8 at 1 Myr (see Fig. 2). The majority of these bound particles perturbed from the disc extent have a semimajor axis larger than the outer edge of the disc, 120 au, while only a small fraction orbit within the inner edge.

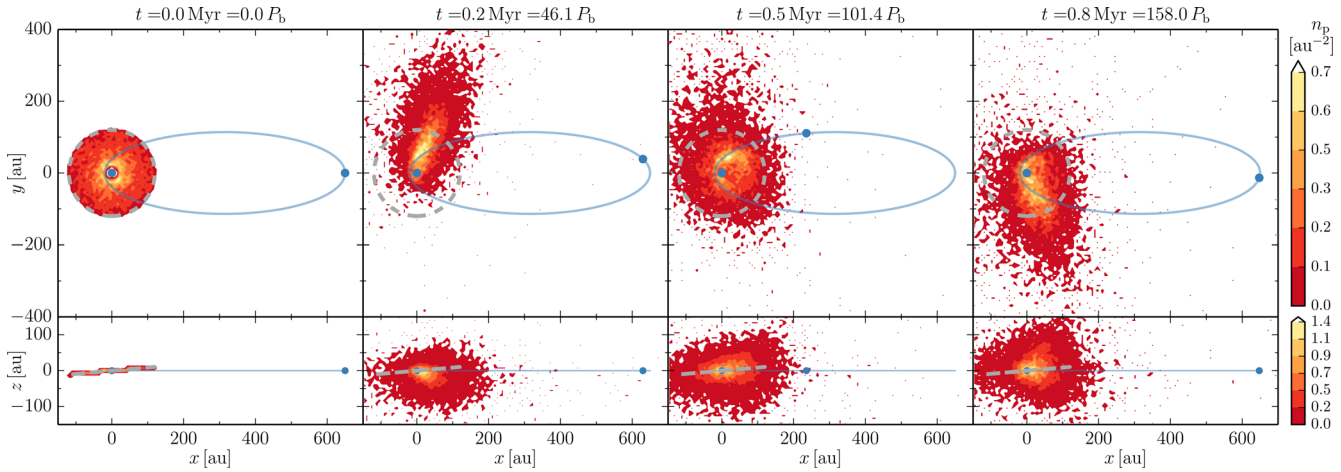

Figure 1. Snapshots from the simulation with $R_{\rm p} = 20$ au and $i = 5°$. The time of the snapshots is indicated above each panel in Myr and in $P_{\rm b}$ (orbital period of the planet). The colour scale maps the number of planetesimals, $n_{\rm p}$, projected in the planetary orbit plane (xy) and the edge-on view of the initial disc (plane perpendicular to the planetary orbit, xz) in the upper and the lower panel, respectively. The star, the planet and its orbit are indicated by the blue points and the solid blue line. The dashed grey ellipse and line segment show the initial extent of the disc. The planet and the planetesimals rotate in the same sense, counterclockwise in the xy plane.

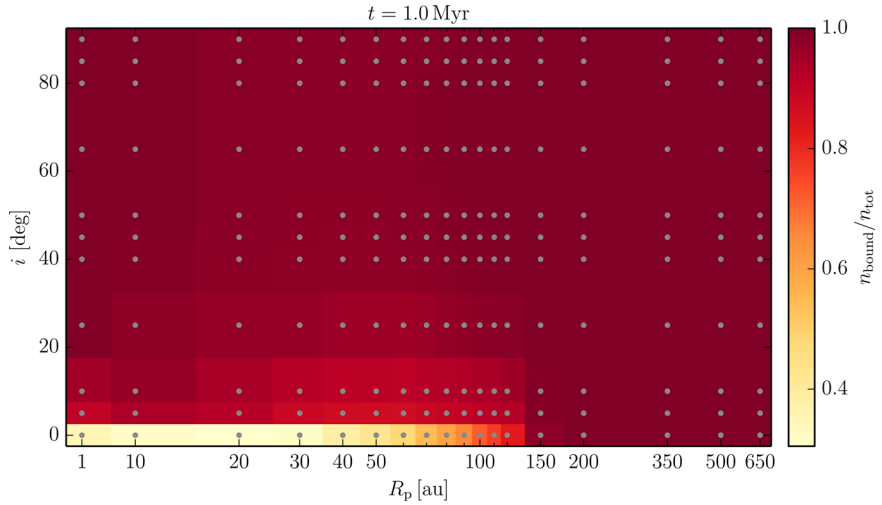

Figure 2. The fraction of particles that stay bound to the star after 1 Myr mapped in the pericentre–inclination plane. The planetary pericentres and disc inclinations are changing along the horizontal and the vertical axis, respectively. The plane is divided into coloured bins and the R_p and i of the grid used are indicated by points. Note that the horizontal axis is logarithmic except for the smallest pericentre (1 au), which is shown on a different scale for clarity.

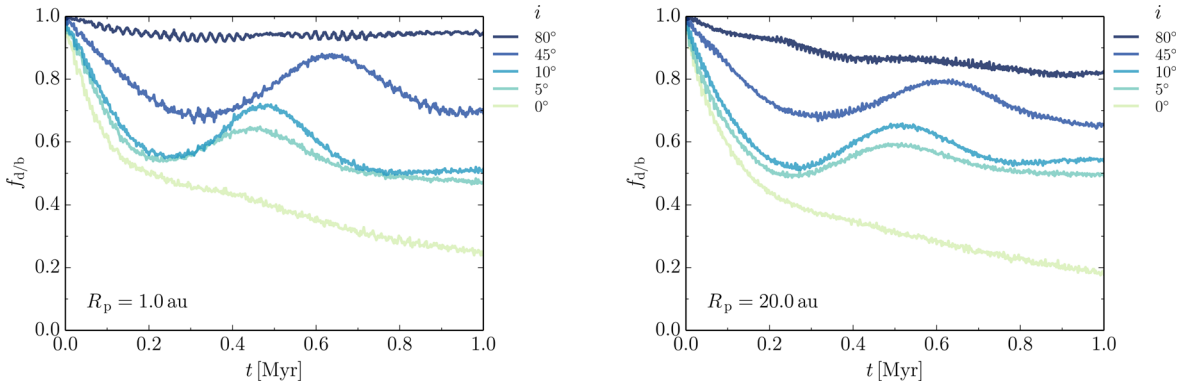

Figure 3. Evolution of the fraction $f_{d/b}(t)$ for pericentre distances of 1 au (left) and 20 au (right) and various inclinations of the disc with respect to the planetary orbit $i < 90^\circ$ (prograde cases). Lines of different colours correspond to different i, as indicated to the right of each plot.

To estimate how consistent our simulations are with the observed disc, we follow the ratio of the number of particles with an instantaneous distance from the star within the observationally constrained disc extent and the number of particles bound to the star. We call this quantity the *disc fraction* $f_{d/b}$ and it is given as $f_{d/b} = n(20\,\mathrm{au} < R < 120\,\mathrm{au})/n_{bound}$, where $n(R)$ is the number of particles at a given distance R (spherical radius) from the star. We use the instantaneous distance because the disc is not resolved in the observations and its extent is estimated from the temperature that is given by the distance of the debris from the star. We tested that in the case when the semimajor axis of the particle orbits is used instead of the instantaneous distance, the evolution of the ratio stays generally similar; however, its modulations, both short- and long-term (see Section 4), are not present.

As mentioned, the ratio $f_{d/b}$ measures the similarity of the simulated system to the observed state. If this ratio is high, most of the particles are orbiting within the radii constrained by observations; a low value of $f_{d/b}$ indicates that most of the particles bound to the star are orbiting outside the constrained radii.

In Fig. 3, we show the evolution of $f_{d/b}$ over 1 Myr for the cases when the pericentre of the planetary orbit is 1 au and when it coincides with the inner edge of the disc ($R_p = 20$ au) for a number of disc inclinations. We focus on the cases with the pericentre within the inner disc edge, because such configurations are expected if the planetary orbit is the result of planet–planet scattering. In both cases, generally the lower the inclination, the lower the ratio $f_{d/b}$ and there is about 30 per cent difference between an inclination of 5° and the coplanar configuration. The evolution of $f_{d/b}(t)$ is not monotonic and is the subject of (at least) two modulations with different time-scales of about 0.05 and 0.3 Myr.

In Fig. 4, we show $f_{d/b}(t)$ for configurations when the disc has a retrograde rotation with respect to the orbit of the planet (i.e. $i \geq 90^\circ$) with a pericentre of 20 au. The evolution of the disc fraction looks generally very similar to the prograde cases with the same planetary pericentre (Fig. 3, right).

Finally, in Fig. 5, we show $f_{d/b}(t)$ for fixed inclinations of 0° and 45° and several values of the pericentre of the planetary orbit. As expected, the disc fraction is generally higher for the configurations with larger pericentres – more than about 80 per cent of particles lie within the disc for pericentres beyond the outer edge, $R_p > 120$ au. Similarly to Figs 3 and 4, the disc fraction oscillates with two

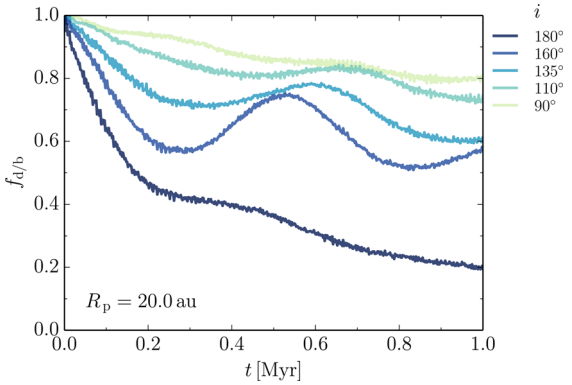

Figure 4. Evolution of the fraction $f_{d/b}(t)$ for a pericentre distance of 20 au and various inclinations of the disc with respect to the planetary orbit $i \geq 90°$ (retrograde cases).

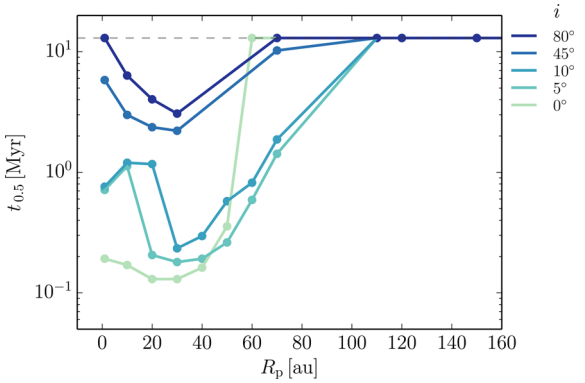

Figure 6. Dependence of $t_{0.5}$, when $f_{d/b}(t_{0.5}) = 0.5$, on the pericentre of the planetary orbit for different inclinations. The dashed horizontal line indicates the lifetime of the system, 13 Myr.

different time-scales – the modulation with the longer time-scale occurs only in cases with non-zero inclination, while the shorter one is present for configurations with higher disc fraction $f_{d/b} \gtrsim 0.7$. A possible explanation for these is discussed in Section 4.

3.2 Disc lifetime

When the ratio $f_{d/b}$ decreases below 0.5, more bound disc particles are located outside than inside the distance range constrained from observations. The moment when $f_{d/b}(t_{0.5}) = 0.5$ can be taken as a measure of the lifetime of the disc as we observe it today. In Fig. 6, we show how $t_{0.5}$ changes with pericentre R_p for different inclinations. Note that, for some of the simulations to obtain $t_{0.5}$ for pericentres $R_p = 1$ and 10 au, 10^3 particles were used rather than the standard 10^4. We tested that this does not change the results (see also Section 2.2). In some configurations, $f_{d/b}(t)$ is not monotonic and the moment when $f_{d/b} = 0.5$ occurs more than once (see Section 4 for a discussion on the oscillations and wobbles); we use the earliest moment to measure $t_{0.5}$ in these cases. Using later times leads to a qualitatively similar plot and does not change the conclusions. Fig. 6 shows $t_{0.5}$ for pericentres up to 150 au; wider pericentres, regardless of the inclination, have $t_{0.5}$ longer than the system lifetime.

The time-scale $t_{0.5}$ is shorter than 1 Myr for configurations with low inclination ($i \lesssim 10°$) and pericentres smaller and close to the inner edge of the disc ($R_p \lesssim 60$ au).

The choice of $f_{d/b} = 0.5$ as the critical value to test for consistency with the observations is arbitrary. The appropriate choice is in principle given by the observational limits (i.e. the minimal detectable mass density of the debris disc). We verified that the general results do not change when considering $f_{d/b}$ in the range 0.3–0.8. As expected, the lower the ratio (i.e. the smaller the fraction of particles within the original disc region), the longer the time-scale.

Values of $f_{d/b}$ at 1 Myr are shown in Fig. 7. Similarly to Fig. 6, more than half of the bound particles are located outside the disc (i.e. $f_{d/b}(1\,\mathrm{Myr}) < 0.5$) for small pericentres and low inclinations. The disc stays relatively unperturbed for $R_p \gtrsim 150$ au, regardless of the inclination.

4 DISCUSSION

4.1 Disc wobbling and Kozai–Lidov-like oscillations

As mentioned in Section 3.2, for some of the configurations with inclined discs, the disc fraction does not decrease monotonically (see Fig. 3). The modulation in $f_{d/b}(t)$ can be explained by a wobbling of the disc. We argue that this wobbling is caused by a mechanism similar to Kozai–Lidov oscillations (Kozai 1962; Lidov 1962).

The Kozai–Lidov mechanism describes the exchange of angular momentum in stable hierarchical three-body systems. The inner binary is periodically excited to high eccentricity and inclination with respect to the initial orbital plane and its argument of periapse librates (i.e. oscillates around a fixed value) with the same period. However, the energy, i.e. the semimajor axis of the orbit, does not change in the standard picture of the Kozai–Lidov mechanism (e.g. Mardling & Aarseth 2001). The amplitude of the oscillations

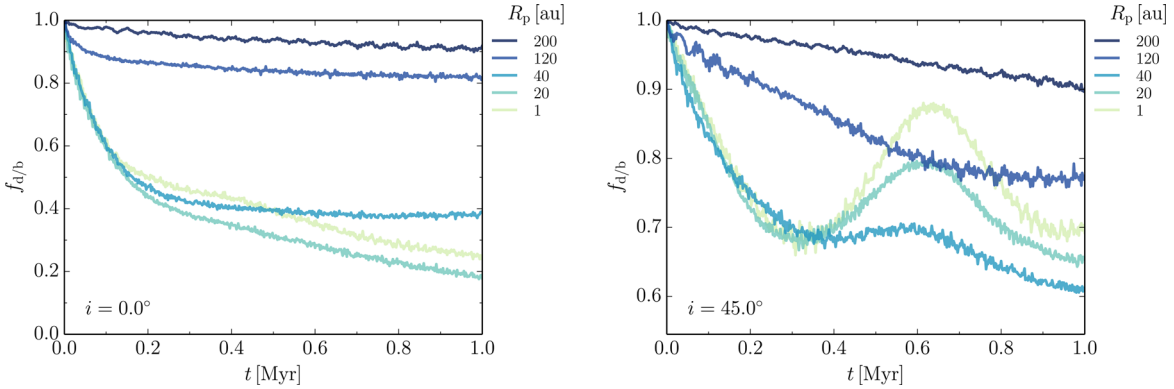

Figure 5. Evolution of the fraction $f_{d/b}(t)$ for disc inclinations of 0° (left) and 45° (right) and various pericentres of the planetary orbit. Lines of different colours correspond to different R_p, as indicated to the right of each plot.

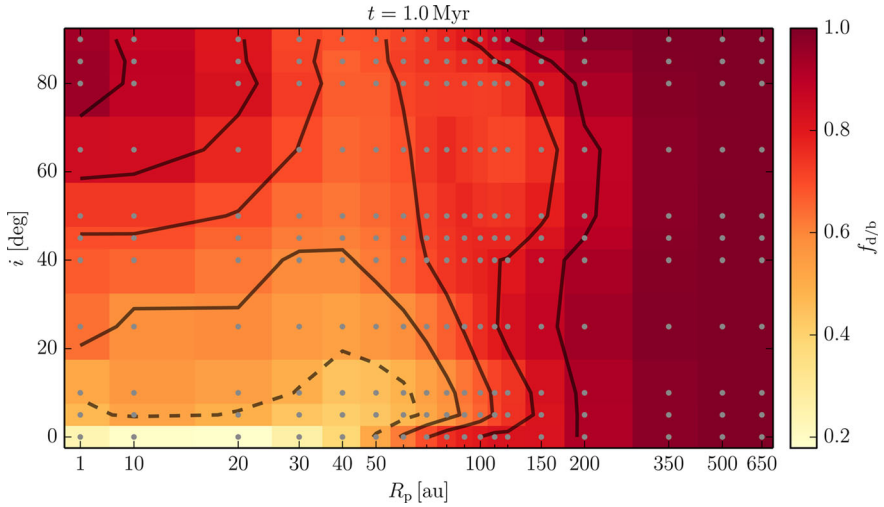

Figure 7. The ratio $f_{\mathrm{d/b}}$ at a time of 1 Myr mapped in the pericentre–inclination plane. The planetary pericentres and disc inclinations are changing along the horizontal and vertical axes, respectively. The plane is divided into coloured bins and the R_{p} and i of the grid used are indicated by points. The colour maps the $f_{\mathrm{d/b}}(1\,\mathrm{Myr})$ for a given configuration of R_{p} and i. The horizontal axis is logarithmic, except for the smallest pericentre (1 au), which is shown on a different scale for clarity. Contour lines are overplotted: their levels start from 0.5 and increase by 0.1; the contour for $f_{\mathrm{d/b}}(1\,\mathrm{Myr}) = 0.5$ is indicated by the dashed line.

depends on the relative inclination of the orbits: the higher the inclination, the bigger the changes of eccentricity (e.g. Innanen et al. 1997). The period of the Kozai–Lidov oscillations depends on the masses of the bodies, the periods of the orbits and the eccentricity of the outer binary.

The Kozai–Lidov time-scale for the restricted three-body problem is approximately given by (see e.g. Hamers et al. 2013, and references therein)

$$T_{\mathrm{KL}} = \alpha \frac{P_{\mathrm{b}}^2}{P_{\mathrm{d}}} \frac{M_\star + M_{\mathrm{b}}}{M_{\mathrm{b}}} \left(1 - e_{\mathrm{b}}^2\right)^{3/2}, \quad (1)$$

where P_{b} and e_{b} are the period and eccentricity of the planetary orbit, respectively. $M_\star$ and M_{b} are the central star and the planet mass, respectively. The orbital period of the disc planetesimal is P_{d}. α is a coefficient of order unity.

The strongest modulation of $f_{\mathrm{d/b}}(t)$ in Fig. 3 happens for the case with $R_{\mathrm{p}} = 1$ au and $i = 45^\circ$. This configuration (and others presented in Fig. 3) does not correspond to the classical Kozai–Lidov example: the planet orbits inside the inner disc radius and the system star–planet–disc particle does not classify as a hierarchical triple. However, since the planetary orbit is very eccentric (an eccentricity of 0.997 for $R_{\mathrm{p}} = 1$ au), the time the planet spends closer to the star than 20 au is extremely short – less than 0.3 per cent of the orbital period – and the time within the outer disc radius of 120 au is about 3.6 per cent of the period. The planet moves outside the disc for most of the time and periodically perturbs the orbits of the disc particles, changing their inclination and eccentricity similarly to the Kozai–Lidov mechanism. At the same time, we do not observe a substantial change in the semimajor axes of planetesimal orbits and modulations of $f_{\mathrm{d/b}}(t)$ are not present when the semimajor axis is used to measure the disc fraction, instead of the instantaneous distance of the particles from the star.

In Fig. 8, we show the dependence of T_{KL} on the pericentre of the planetary orbit R_{p} (i.e. on e_{b} and P_{b}) for different semimajor axes of the planetesimals R_{d} (i.e. different P_{d}). T_{KL} for R_{p} between 1 au and 20 au ranges from about 0.004–1 Myr depending on R_{d}. Wobbles happen on a time-scale of ∼0.1 Myr, which is generally consistent (considering the factor α) with the T_{KL} for the particles

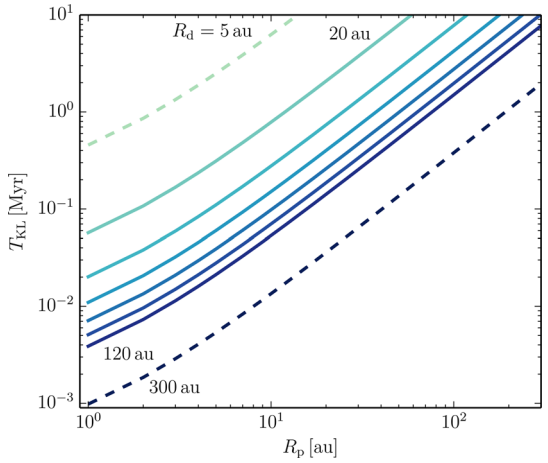

Figure 8. Time-scale of the Kozai–Lidov mechanism, T_{KL}, as given by equation (1), as a function of the pericentre of the planetary orbit, R_{p}. Different lines show the dependence for different semimajor axes of the disc planetesimals, R_{d}. Several values of R_{d} are indicated in the plot. Dashed lines show cases when R_{d} is outside the initial disc, while full lines show cases within the initial disc with a step size of 20 au.

in the inner parts of the disc and pericentre $R_{\mathrm{p}} \sim$ 1–5 au and the full radial range of the disc for larger R_{p}.

We suggest that the combination of the perturbation of planetesimal orbits and a mechanism similar to the Kozai–Lidov oscillations leads to wobbling of the disc, when the eccentricities, inclinations and argument of periapse (i.e. the orientation of the orbits) change for a number of disc planetesimals. We illustrate the process in Fig. 9, where we show snapshots of the simulation with the planetary pericentre at 1 au and a disc inclination of 45°. The four snapshots show the initial state of the system and times close to the minima ($t = 0.3$ and 0.9 Myr) and maximum ($t = 0.6$ Myr) of the $f_{\mathrm{d/b}}(t)$ modulation (see Fig. 3). At $t = 0.3$ and 0.9 Myr, the particles are collectively perturbed to higher inclinations and eccentricities and the plane of the disc is close to perpendicular to the orbital plane of the planet, while at $t = 0.6$ Myr the disc has a configuration

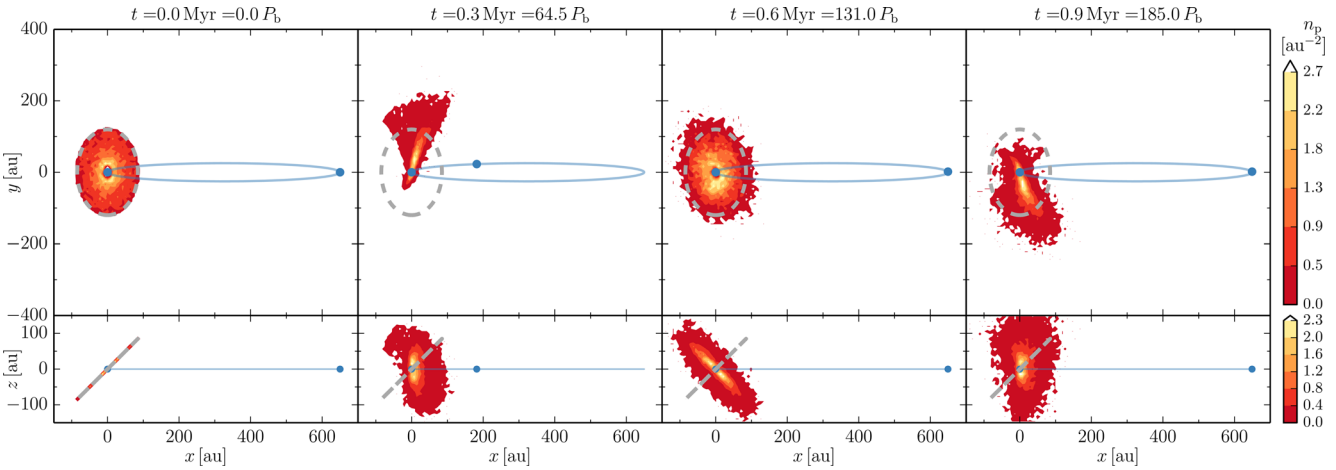

Figure 9. Snapshots from the simulation with $R_p = 1$ au and $i = 45°$; see Fig. 1 for a detailed description.

similar to that at the beginning, but with retrograde rotation (an inclination of about $-45°$).

4.2 Short-term oscillations of $f_{d/b}$

Apart from the modulation on the time-scales of ∼0.1 Myr, the disc fractions $f_{d/b}(t)$ show periodical modulations with amplitudes $\lesssim$0.03 and time-scales $\lesssim$0.05 Myr for most configurations (see Figs 3 and 5, especially the cases with higher disc fractions). The modulation results from resonant spiral density waves and rings induced by the planet in the disc. If a resonant radius is located close to the initial outer edge of the disc, a certain number of planetesimals orbit periodically just inside or outside the disc. The modulation is most prominent for cases when the relative mass is $f_{d/b} \gtrsim 0.7$ and the resonant patterns are stable enough. If such resonant features are resolved by future observations, they could provide constraints on the orbit of the planet.

5 CONCLUSIONS

We studied the lifetime of the debris disc in the peculiar system HD 106906. This 13-Myr old star is orbited by a debris disc and a planetary-mass companion at a separation of 650 au. We carried out simulations of the system using the AMUSE environment. Since the disc is much less massive than the star or the planet, we represent its planetesimals by zero-mass particles. We implemented a hybrid numerical method in which the orbit of the planet is solved independently of the disc and the disc planetesimals are integrated in the potential of the star and the planet. The initial conditions for the simulations were given by the observed characteristics of the system and the unconstrained characteristics of the system – namely the pericentre distance of the planetary orbit and the inclination of the disc with respect to the planetary orbit – were varied systematically.

We find that more than 80 per cent of the disc particles stay bound to the star for the majority of configurations considered and only in the case of orbits with low inclination $\lesssim 10°$ and pericentres of the planetary orbit $\lesssim$50 au is a substantial part of the disc lost during the first 1 Myr of evolution. To estimate how long the disc stays in a configuration consistent with the observations, we followed the ratio of the number of disc particles with distance within the constrained disc radii (20–120 au) and the number of particles bound to the system. We define the lifetime of the disc as the time until more particles are orbiting outside the constrained disc radius than within it (i.e. more particles are at distances <20 au or >120 au than within 20–120 au from the star). The lifetime of the disc is shorter than 1 Myr for orbits with low inclination $i < 5°$ and comparable with 1 Myr when $i \sim 5$–$10°$, with pericentre smaller than or close to the inner edge of the disc ($R_p \lesssim 50$ au, see Figs 6 and 7). Such orbits are expected in the case when the planet formed closer to the star, most probably within the inner disc edge, where it cleared the inner region and was scattered to its current orbit by other members of the system. However, such interaction is estimated to occur during the first 10 Myr of the lifetime of planetary systems (e.g. Veras et al. 2009; Scharf & Menou 2009). Considering the current age of the system of 13 ± 2 Myr (Pecaut et al. 2012), we conclude that configurations with lifetimes shorter than 1 Myr ($i \lesssim 10°$ and $R_p \lesssim 50$ au) are inconsistent with the scenario according to which the current orbit resulted from planet–planet scattering from the inner disc.

When the disc is inclined with respect to the planetary orbit with inclination $\gtrsim 40°$, it can survive longer than 1 Myr even in the case in which the pericentre is within the inner disc edge. In these configurations, the disc wobbles (see Fig. 8). We argue that this is caused by a mechanism similar to the Kozai–Lidov oscillations induced by the planet on the disc particles. The planet can also induce resonant structures in the disc, such as spiral arms and rings.

ACKNOWLEDGEMENTS

We thank the anonymous referee for reviewing our work and for insightful comments that improved the manuscript. We thank Guilherme Gonçalves Ferrari, Inti Pelupessy and Tjarda Boekholt for their help with the Kepler solver used in our numerical method. We thank Adrian Hamers for enriching discussions about the Kozai–Lidov mechanism and Matthew Kenworthy and Tiffany Meshkat for discussions about HD 106906. We thank Gráinne Costigan for reading the manuscript and for her useful comments. This work was supported by the Interuniversity Attraction Poles Programme initiated by the Belgian Science Policy Office (IAP P7/08 CHARM), the Netherlands Research Council NWO (grants #643.200.503, #639.073.803 and #614.061.608) and the Netherlands Research School for Astronomy (NOVA).

REFERENCES

Andrews S. M., Williams J. P., 2007, ApJ, 659, 705
Bailey V. et al., 2014, ApJ, 780, L4
Baruteau C. et al., 2014, in Beuther H., Klessen R. S., Dullemond C. P., Henning T., eds, Protostars and Planets VI, Vol. 914, Univ. Arizona Press, Tucson, p. 667
Boley A. C., Payne M. J., Ford E. B., 2012, ApJ, 754, 57
Boss A. P., 2011, ApJ, 731, 74
Chabrier G., Johansen A., Janson M., Rafikov R., 2014, in Beuther H., Klessen R. S., Dullemond C. P., Henning T., eds, Protostars and Planets VI, Vol. 914, Univ. Arizona Press, Tucson, p. 619
Chatterjee S., Ford E. B., Matsumura S., Rasio F. A., 2008, ApJ, 686, 580
Chen C. H., Jura M., Gordon K. D., Blaylock M., 2005, ApJ, 623, 493
Chen C. H., Mamajek E. E., Bitner M. A., Pecaut M., Su K. Y. L., Weinberger A. J., 2011, ApJ, 738, 122
Chiang E., Kite E., Kalas P., Graham J. R., Clampin M., 2009, ApJ, 693, 734
Crida A., Masset F., Morbidelli A., 2009, ApJ, 705, L148
D'Angelo G., Durisen R. H., Lissauer J. J., 2011, in Seager S., ed., Exoplanets. University of Arizona Press, Tucson, AZ, p. 319
Davies M. B., Adams F. C., Armitage P., Chambers J., Ford E., Morbidelli A., Raymond S. N., Veras D., 2014, in Beuther H., Klessen R. S., Dullemond C. P., Henning T., eds, Protostars and Planets VI, Vol. 914, Univ. Arizona Press, Tucson, p. 787
de Zeeuw P. T., Hoogerwerf R., de Bruijne J. H. J., Brown A. G. A., Blaauw A., 1999, AJ, 117, 354
Faramaz V. et al., 2014, A&A, 563, 72
Fujii M., Iwasawa M., Funato Y., Makino J., 2007, PASJ, 59, 1095
Gonçalves Ferrari G., Boekholt T., Portegies Zwart S. F., 2014, MNRAS, 440, 719
Hamers A. S., Pols O. R., Claeys J. S. W., Nelemans G., 2013, MNRAS, 430, 2262
Hao W., Kouwenhoven M. B. N., Spurzem R., 2013, MNRAS, 433, 867
Hayashi C., 1981, Progr. Theor. Phys. Suppl., 70, 35
Innanen K. A., Zheng J. Q., Mikkola S., Valtonen M. J., 1997, AJ, 113, 1915
Kozai Y., 1962, AJ, 67, 591
Kraus A. L., Ireland M. J., Cieza L. A., Hinkley S., Dupuy T. J., Bowler B. P., Liu M. C., 2014, ApJ, 781, 20
Lafreniere D., Jayawardhana R., van Kerkwijk M. H., 2008, ApJ, 689, L153
Larwood J. D., Kalas P. G., 2001, MNRAS, 323, 402
Lestrade J.-F., Morey E., Lassus A., Phou N., 2011, A&A, 532, 120
Lidov M. L., 1962, Planet. Space Sci., 9, 719
Malmberg D., Davies M. B., Heggie D. C., 2011, MNRAS, 411, 859
Mardling R. A., Aarseth S. J., 2001, MNRAS, 321, 398
Naud M.-E. et al., 2014, ApJ, 787, 5
Pearce T. D., Wyatt M. C., 2014, MNRAS, 443, 2541
Pecaut M. J., Mamajek E. E., Bubar E. J., 2012, ApJ, 746, 154
Pelupessy F. I., Jänes J., Portegies Zwart S., 2012, New Astron., 17, 711
Pelupessy F. I., van Elteren A., de Vries N., McMillan S. L. W., Drost N., Portegies Zwart S. F., 2013, A&A, 557, 84
Perets H. B., Kouwenhoven M. B. N., 2012, ApJ, 750, 83
Portegies Zwart S., Boekholt T., 2014, ApJ, 785, L3
Portegies Zwart S. F., McMillan S. L. W., 2005, ApJ, 633, L141
Portegies Zwart S., McMillan S. L. W., van Elteren E., Pelupessy I., de Vries N., 2013, Comput. Phys. Commun., 183, 456
Rafikov R. R., 2011, ApJ, 727, 86
Raymond S. N., Armitage P. J., Gorelick N., 2010, ApJ, 711, 772
Rebull L. M., Stauffer J. R., Megeath S. T., Hora J. L., Hartmann L., 2006, ApJ, 646, 297
Reche R., Beust H., Augereau J.-C., Absil O., 2008, A&A, 480, 551
Scharf C., Menou K., 2009, ApJ, 693, L113
Steinhausen M., Olczak C., Pfalzner S., 2012, A&A, 538, A10
Thébault P., 2012, A&A, 537, 65
van Leeuwen F., 2007, A&A, 474, 653
Veras D., Evans N. W., 2013, MNRAS, 430, 403
Veras D., Crepp J. R., Ford E. B., 2009, ApJ, 696, 1600
Vorobyov E. I., 2013, A&A, 552, 129
Wisdom J., Holman M., 1991, AJ, 102, 1528
Wyatt M. C., 2003, ApJ, 598, 1321
Wyatt M. C., 2008, ARA&A, 46, 339

This paper has been typeset from a TEX/LATEX file prepared by the author.